PHYSICAL REVIEW C **86**, 041303(R) (2012)

Reorientation-effect measurement of the $\langle 2_1^+ \| \hat{E}2 \| 2_1^+ \rangle$ matrix element in ^{10}Be

J. N. Orce,[1,2,*] T. E. Drake,[3] M. K. Djongolov,[1] P. Navrátil,[1,4] S. Triambak,[1,5] G. C. Ball,[1] H. Al Falou,[1,6] R. Churchman,[1] D. S. Cross,[7] P. Finlay,[8] C. Forssén,[9] A. B. Garnsworthy,[1] P. E. Garrett,[8] G. Hackman,[1] A. B. Hayes,[10] R. Kshetri,[1,7] J. Lassen,[1] K. G. Leach,[8] R. Li,[1] J. Meissner,[1] C. J. Pearson,[1] E. T. Rand,[8] F. Sarazin,[11] S. K. L. Sjue,[1] M. A. Stoyer,[4] C. S. Sumithrarachchi,[8] C. E. Svensson,[8] E. R. Tardiff,[1] A. Teigelhoefer,[1] S. J. Williams,[1,†] J. Wong,[8] and C. Y. Wu[4]

[1]*TRIUMF, 4004 Wesbrook Mall, Vancouver, British Columbia V6T 2A3, Canada*
[2]*Department of Physics, University of the Western Cape, P/B X17, Bellville ZA-7535, South Africa*
[3]*Department of Physics, University of Toronto, Toronto, Ontario M5S 1A7, Canada*
[4]*Lawrence Livermore National Laboratory, Livermore, California 94550, USA*
[5]*Department of Physics and Astrophysics, University of Delhi, Delhi 110 007, India*
[6]*Astronomy and Physics Department, Saint Mary's University, Halifax NS B3H 3C3, Canada*
[7]*Department of Chemistry, Simon Fraser University, Burnaby, British Columbia V5A 1S6, Canada*
[8]*Department of Physics, University of Guelph, Guelph, Ontario N1G 2W1, Canada*
[9]*Fundamental Physics, Chalmers University of Technology, SE-412 96 Göteborg, Sweden*
[10]*Department of Physics and Astronomy, University of Rochester, Rochester, New York 14627, USA*
[11]*Physics Department, Colorado School of Mines, Golden, Colorado 80401, USA*

(Received 30 January 2012; revised manuscript received 31 August 2012; published 17 October 2012)

The highly-efficient and segmented TIGRESS γ-ray spectrometer at TRIUMF has been used to perform a reorientation-effect Coulomb-excitation study of the 2_1^+ state at 3.368 MeV in ^{10}Be. This is the first Coulomb-excitation measurement that enables one to obtain information on diagonal matrix elements for such a high-lying first excited state from γ-ray data. With the availability of accurate lifetime data, a value of -0.110 ± 0.087 eb is determined for the $\langle 2_1^+ \| \hat{E}2 \| 2_1^+ \rangle$ diagonal matrix element, which assuming the rotor model, leads to a negative spectroscopic quadrupole moment of $Q_s(2_1^+) = -0.083 \pm 0.066$ eb. This result is in agreement with both no-core shell-model calculations performed in this work with the CD-Bonn 2000 two-nucleon potential and large shell-model spaces, and Green's function Monte Carlo predictions with two- plus three-nucleon potentials.

DOI: 10.1103/PhysRevC.86.041303 PACS number(s): 21.10.Re, 21.60.Cs, 23.20.−g, 27.20.+n

Modern nuclear theory provides numerical methods to solve the nonrelativistic Schrödinger equation for light nuclear systems [1,2]. Wave functions of nuclear states can be derived from a large-scale diagonalization in the no-core shell model (NCSM) [1] and from variational Monte Carlo methods [2], enabling nuclear-structure properties to be calculated from *ab initio* or first principles. While excitation energies [1,3,4] and charge radii [5–7] are generally reproduced with high accuracy, agreement with the experimental data often requires very large shell-model space sizes [8,9] and the inclusion of three-nucleon ($3N$) forces in the full Hamiltonian [3,10,11]. Major recent breakthroughs of *ab initio* calculations include the reproduction of the Hoyle state [12], and the computation of fusion-reaction cross sections relevant to big bang nucleosynthesis and fusion-energy research [13]. With respect to excitation energies and charge radii, electromagnetic-multipole matrix elements can potentially provide more stringent tests of wave functions because of the overlap between initial and final nuclear states.

The nucleus ^{10}Be is an important testing ground for *ab initio* calculations of electric-quadrupole matrix elements [8,14,15]. The precise lifetime recently measured for the 2_1^+ state at 3.368 MeV has underlined the relevance of constraining and constructing better-quality $3N$ potentials [15]. A reduced attraction of the spin-orbit interaction in the $IL7(3N)$ Hamiltonian leads to a better reproduction of energies and transitional matrix elements in Green's function Monte Carlo (GFMC) calculations. Stronger evidence regarding the effect of $3N$ forces in ^{10}Be is the reordering of nuclear levels predicted by GFMC calculations. As opposed to using only the $AV_{18}(2N)$ potential, a reversed level ordering for the first two $J^\pi = 2^+$ excited states is predicted by including the $IL2(3N)$ potential [14]. Excitation energies of these $J^\pi = 2^+$ states calculated with the NCSM and the CD-Bonn 2000($2N$) potential [8] obtain the same ordering as the GFMC calculations with the $AV_{18}(2N)$ plus the $IL2(3N)$ interactions. This is probably because of the stronger spin-orbit interaction generated by the CD-Bonn 2000 potential, which is a nonlocal interaction based on a boson-exchange picture, as compared with the local $AV_{18}(2N)$ interaction [8]. Nonetheless, GFMC calculations with the $AV_{18}(2N) + IL7(3N)$ Hamiltonian provide an experimental means to test the reordering of the 2^+ levels by predicting different signs for their *spectroscopic quadrupole moment* (Q_s) of the nuclear charge distribution in the laboratory frame; that is, $Q_s(2_1^+)_{\rm GFMC} = -0.067(1)$ eb and $Q_s(2_2^+)_{\rm GFMC} = +0.045(1)$ eb [16].

In this work, we test these predictions with a Coulomb-excitation measurement of the $\langle 2_1^+ \| \hat{E}2 \| 2_1^+ \rangle$ diagonal matrix element of the electric-quadrupole tensor in ^{10}Be. New NCSM calculations of matrix elements involving the 2_1^+ and 2_2^+ states in ^{10}Be, as well as nuclear polarizabilities for the ground state

*coulex@gmail.com; http://www.pa.uky.edu/∼jnorce
†Present address: NSCL, Michigan State University, East Lansing, Michigan 48824, USA.

of ^{9}Be and 2_1^+ state in ^{10}Be, are also presented. Further details of both experimental results and the theoretical calculations will be given in a separate paper [17].

A Coulomb-excitation study of radioactive ^{10}Be (with a half-life of 1.51×10^6 years) has been carried out at energies well below the Coulomb barrier at the TRIUMF/ISAC-II radioactive-ion-beam facility. A tantalum primary fragmentation/spallation target was bombarded by a 500-MeV, 40-μA proton beam from the TRIUMF main cyclotron to produce radioactive ^{10}Be. Singly charged ^{10}Be ions were extracted using the TRIUMF Resonant Ionization Laser Ion Source (TRILIS) [18]. Following mass separation the isotopically pure ^{10}Be beam was further stripped to a 2^+ charge state before acceleration to a projectile kinetic energy of $T_p = 41$ MeV. The beam was made to impinge on a 3.0 mg/cm^2 ^{194}Pt target (96.5% enriched) at the center of the TIGRESS γ-ray spectrometer [19]. An average intensity of $\approx 1.1 \times 10^7$ ^{10}Be ions/s was maintained for a period of four days.

Gamma rays emitted following the de-excitation of states in the beam and target nuclei were detected by eight segmented, highly efficient, Compton-suppressed TIGRESS clover detectors positioned 152 mm from the target and covering approximately 15% of 4π. Each clover is comprised of four eight-fold segmented high-purity germanium (HPGe) crystals surrounded by a 20-fold segmented Compton suppression shield [20,21]. Scattered ^{10}Be ions were detected using an annular, double-sided CD-type silicon detector comprised of 32 sectors and 24 rings. This detector was mounted downstream at 19.4 mm from the target, aligned perpendicular to the beam axis and subtending laboratory polar angles between 30.6° and 61.0°. The scattered beam was fully stopped in the 500-μm thick silicon detector.

Background γ rays from the experimental hall and beam-dump were suppressed by requiring a particle-γ coincidence condition, i.e., the combination of a TIGRESS hit and a hit in both the θ ring and ϕ sector of the Si detector within a time window of 195 ns. The relative angle between the registered particle in the silicon detector and the γ ray was determined using the geometric center of the hit segment in the TIGRESS clovers. In the case of multiple crystals triggering in the same module, the crystal with the highest deposited energy was identified and the center of the segment with the highest energy within that crystal was used to Doppler correct the add-back energy.

Typical particle energy spectra at ring angles of $\theta = 35.6°$ and 60.0° are shown in Fig. 1. Particle spectra were calibrated utilizing α sources of ^{239}Pu, ^{241}Am, and ^{244}Cm together with kinematics considerations for the scattered ^{10}Be ions; including energy losses in the ^{194}Pt target and the 0.58-mg/cm^2 thick ^{197}Au coating on the silicon strips [24]. An additional particle-energy condition, $|E_{\rm ring} - E_{\rm sector}| \leqslant 350$ keV, was applied to account for the energy sharing between the rings and sectors and dead layers in the Si detector. The 350 keV restriction was varied to assure no 3368 keV peak counts were lost. As shown in Fig. 1, this energy condition reduced the background in the low- and intermediate-energy regions of the particle spectra enabling a better selection of the ^{10}Be inelastically scattered particle [17]. The same energy-sharing condition as well as a broad particle-energy gate, which included both inelastic and elastic peaks, were employed to ensure full collection of the 328 keV γ-ray transition in ^{194}Pt. The resulting γ-ray energy spectra is shown in Fig. 2.

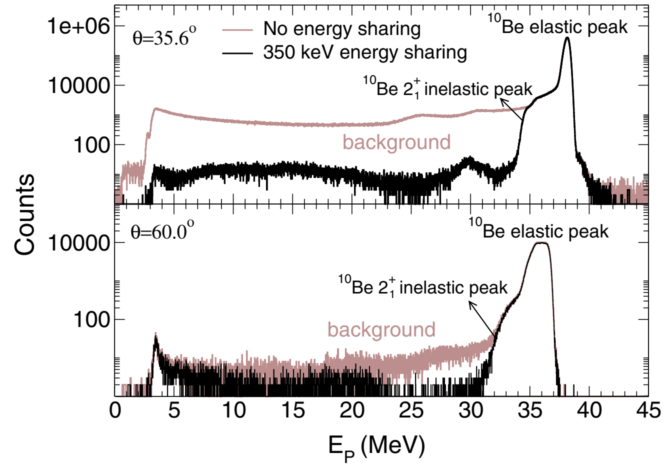

FIG. 1. (Color online) Particle-energy spectrum for rings at average angles of $\theta = 35.6°$ (top panel) and 60.0° (bottom panel). The application of $|E_{\rm ring} - E_{\rm sector}| \leqslant 350$ keV permits a good identification of the 2_1^+ inelastic peak in ^{10}Be. The larger background at $\theta = 35.6$ arises from the higher density of dead layers for innermost rings in the silicon detector.

The Q_s values of excited states with angular momenta $J \neq 0, \frac{1}{2}$ can be determined in Coulomb-excitation reactions using the *reorientation effect* (RE), a second-order perturbation that generates a time-dependent hyperfine splitting of the nuclear levels and changes the population of the different magnetic substates; hence, modifying the Coulomb-excitation cross section according to the magnitude and sign of Q_s [25].

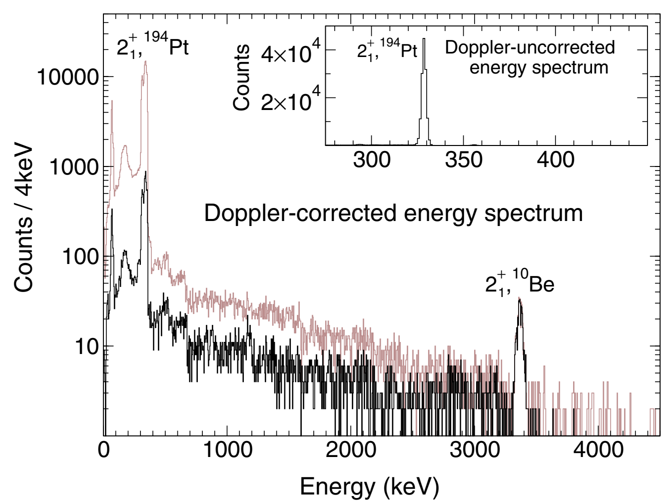

FIG. 2. (Color online) Gamma-ray energy spectra for the ^{194}Pt(^{10}Be,^{10}Be*)^{194}Pt* reaction at 41 MeV. The main panel shows Doppler-corrected energy spectra with (black) and without (brown) a ^{10}Be inelastic-particle-coincidence condition. The former results in a cleaner background, yet conserves the number of counts for the 3.368 MeV transition depopulating the 2_1^+ state in ^{10}Be. The inset shows a Doppler-uncorrected γ-ray spectrum with the 2_1^+ peak at 328 keV in ^{194}Pt.

The use of reactions with negligible nuclear contributions is fundamental in such experiments to avoid Coulomb-nuclear interference [25,26]. Systematic RE studies of light nuclei suggest a minimum separation between nuclear surfaces of $S(\theta)_{\min} \approx 6.4$ fm to obtain consistent Q_s values [25–31]. For the ^{194}Pt(^{10}Be,^{10}Be*)^{194}Pt* reaction at 41 MeV, the laboratory solid angle subtended by the front silicon detector corresponded to even more conservative values of $S(\theta)_{\min} = 6.8$ fm at 61.0°.

The Coulomb-excitation analysis has been performed with the semiclassical coupled-channel Coulomb-excitation least-squares code, GOSIA [32]. In light nuclei, another second-order effect that may influence both the magnitude and sign of diagonal matrix elements is the virtual electric-dipole excitations of states around the giant dipole resonance (GDR) [25,33,34]. Because of the large $E1$ matrix elements, two-step processes of the type $0_1^+ \to 1_{\mathrm{GDR}}^- \to 2_1^+$ may polarize the shape of the 2_1^+ state and affect the determination of $Q_s(2_1^+)$. The GOSIA code accounts for this correction by multiplying the total quadrupole interaction, $V_0(t)$, by a factor of $(1 - z\frac{a}{r})$; where a is the half distance of closest approach, r the magnitude of the projectile-target position vector, and $z = 0.00563k\frac{T_P A_P}{Z_P^2(1+A_P/A_T)}$ [33]; with $A_{P,T}$ being the projectile and target mass numbers and k the *polarizability parameter* [32].

For the case of arbitrary spins, k can be inferred in terms of $E1$ and $E2$ matrix elements [29] from the ratio $k = \frac{X}{X_0}$, where $X_0 = 0.00058\frac{A}{Z}$ $e\mathrm{MeV}^{-1}$ arises from a global fit to the available photoabsorption cross sections [35,36] and X is given by

$$X = \frac{S(E1)}{\langle i\|\hat{E}2\|f\rangle} = \frac{\sum_n W(11J_iJ_f,2J_n)\frac{\langle i\|\hat{E}1\|n\rangle\langle n\|\hat{E}1\|f\rangle}{E_n-E_i}}{\langle i\|\hat{E}2\|f\rangle}, \quad (1)$$

where the sum extends over all intermediate states $|n\rangle$ connecting the initial $|i\rangle$ and final $|f\rangle$ states with $E1$ transitions. Shell model calculations have been successful in reproducing k values for ground and excited states in p shell nuclei [29,37].

In the present work, NCSM calculations using the CD-Bonn 2000 $2N$ potential have been performed to estimate the nuclear polarizability of the 2_1^+ state in ^{10}Be. The known photoabsorption cross section in ^{9}Be of $\sigma_{-2} = 370$ μb/MeV [36,38] corresponds to a large ground-state value of k(g.s.) = 2.7. From an equation analogous to Eq. (1) [37], $k(\mathrm{g.s.})_{\mathrm{NCSM}} = 2.3$ is computed in reasonable agreement with the experimental value. These *ab initio* calculations consider model spaces with basis sizes of $N_{\max} = 4$ and $N_{\max} = 5$ for natural and unnatural parity states, respectively, $\hbar\Omega = 12$ MeV and $E1$ contributions from about CD-Bonn 2000 intermediate $1/2^+$, $3/2^+$, and $5/2^+$ states. For the 2_1^+ state in ^{10}Be, a smaller $k(2_1^+)_{\mathrm{NCSM}} = 0.81$ is predicted from Eq. (1) using $E1$ contributions from all the $J^\pi = 1^-$ states up to 30 MeV. A value of $k(2_1^+)_{\mathrm{NCSM}} = 0.81(20)$ was used in the GOSIA calculations, where the adopted 25% theoretical uncertainty is significantly larger than the 15% difference between the theoretical and experimental values for k(g.s.) in ^{9}Be.

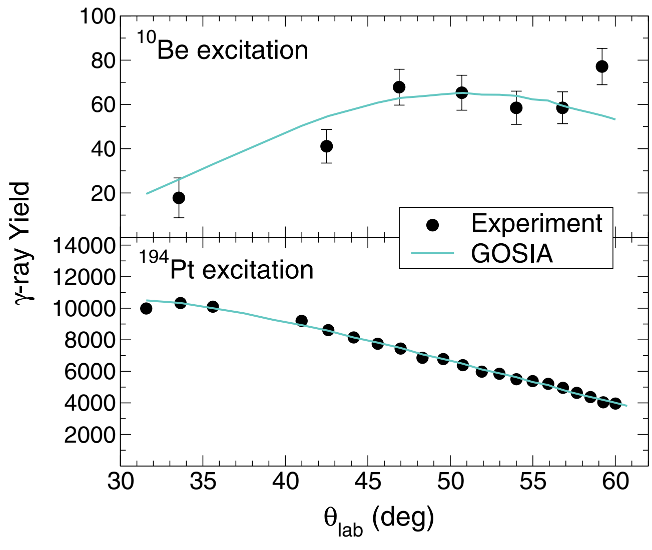

FIG. 3. (Color online) Angular distributions showing experimental and calculated γ-ray yields as a function of particle angle (in the laboratory frame) for the de-excitation of the 2_1^+ states in ^{10}Be (top) and ^{194}Pt (bottom).

The angular distributions of the eight clover yields for the lowest 2^+ states in ^{10}Be and ^{194}Pt are shown in Fig. 3. Since the ^{10}Be 2_1^+ distribution had low statistics, the $\langle 2_1^+\|\hat{E}2\|0_1^+\rangle$ and $\langle 2_1^+\|\hat{E}2\|2_1^+\rangle$ matrix elements were determined from the ratio of the integrated yields [39] of the 3.368 MeV γ ray in ^{10}Be and the 328.5 keV γ ray in ^{194}Pt. Integrated yields were calculated with GOSIA and normalized to the experimental yields. As shown in Fig. 3, the shape of the angular distribution predicted by GOSIA for both ^{10}Be and ^{194}Pt are in good agreement with experiment. The theoretical yields shown in Fig. 3 were calculated using $\langle 2_1^+\|\hat{E}2\|0_1^+\rangle = 0.069$ eb and $\langle 2_1^+\|\hat{E}2\|2_1^+\rangle = -0.110$ eb, i.e., the intersection point of the centroid of the two bands in Fig. 4. In the GOSIA integration of γ-ray yields, angular limits, bombarding energy, and stopping-power mesh points account for the solid angle subtended by the silicon detector and the energy loss of the beam through the target thickness. Further corrections include the γ-ray efficiencies for eight TIGRESS clovers measured using known ^{152}Eu, ^{133}Ba, ^{60}Co, and ^{56}Co calibration sources [17], internal-pair formation processes [40] and angular-distribution attenuation factors for the finite size of the detectors [22,32]. The integrated yield calculations were constrained with available spectroscopic information concerning level lifetimes, branching ratios and matrix elements for all significant couplings up to the 4_2^+ state in ^{194}Pt [41] and the 2_1^+ state in ^{10}Be [15,42,43]. The effect of higher-order couplings in ^{10}Be and ^{194}Pt is negligible.

The calculated integrated yields for projectile, Y_{calc}^P, and target, Y_{calc}^T, are related by $Y_{\mathrm{calc}}^T/Y_{\mathrm{calc}}^P = 1.036N_\gamma^T/N_\gamma^P$; where the factor 1.036 accounts for the 96.5% enrichment of the ^{194}Pt target and N_γ^T and N_γ^P are the experimental number of counts for target and projectile, respectively. Total experimental yields of 386(22) and 141 545(380) counts are observed for the 3,368- and 328-keV γ rays depopulating the 2_1^+ states in ^{10}Be and ^{194}Pt, respectively. The statistical uncertainty of 5.4% from the measured 3,368-keV peak area dominates the quoted error on

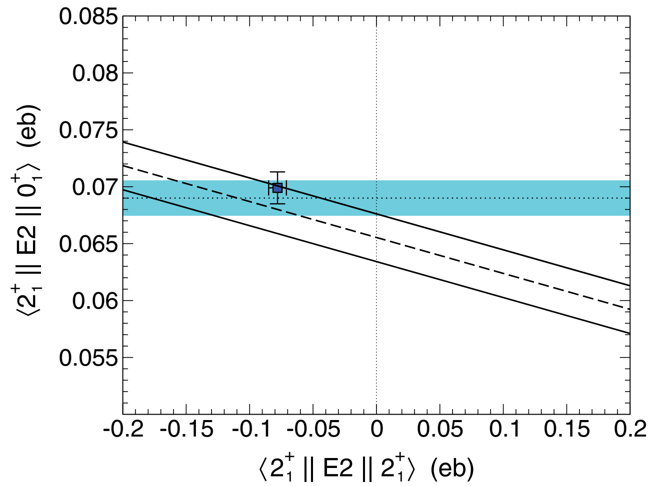

FIG. 4. (Color online) The parabolic lines indicate the central value (dashed) and 1-σ limits (solid) of $\langle 2_1^+ \| \hat{E}2 \| 0_1^+ \rangle$ versus $\langle 2_1^+ \| \hat{E}2 \| 2_1^+ \rangle$ matrix elements in ^{10}Be for $k(2_1^+) = 0.81$. The horizontal band represents the 1-σ boundary for $\langle 2_1^+ \| \hat{E}2 \| 0_1^+ \rangle = 0.0690(15)$ [15,42,43]. The extrapolated NCSM results are given by the square data point; see the text for details.

this measurement. Other contributions include $\langle 2_1^+ \| \hat{E}2 \| 0_1^+ \rangle = 1.281 \pm 0.009$ eb in ^{194}Pt [44,45], which gives an error in the cross section of $\pm 1.4\%$, the spread in polarizability $k = 0.81 \pm 0.20$, γ-ray efficiencies $\approx 2.5\%$, and the ϕ asymmetry of the TIGRESS detectors, $< 0.5\%$ [22,23]. Doppler-shift effects on the γ-ray efficiency are negligible for the 3.368 MeV region.

The variation of $\langle 2_1^+ \| \hat{E}2 \| 0_1^+ \rangle$ as a function of $\langle 2_1^+ \| \hat{E}2 \| 2_1^+ \rangle$ for $k(2_1^+) = 0.81$ in ^{10}Be is represented by the diagonal band in Fig. 4. Data points in the Coulomb-excitation curve (a dashed line for the central value and solid lines for the 1-σ limits) are obtained by fixing $\langle 2_1^+ \| \hat{E}2 \| 2_1^+ \rangle$ and determining the corresponding value of $\langle 2_1^+ \| \hat{E}2 \| 0_1^+ \rangle$ required to obtain the experimental ratio of the γ-ray yields. The horizontal band in Fig. 4 represents the 1-σ boundary for $\langle 2_1^+ \| \hat{E}2 \| 0_1^+ \rangle = 0.0690(15)$ eb as derived from previous lifetime measurements [15,42,43]. Assuming no uncertainty in $\langle 2_1^+ \| \hat{E}2 \| 0_1^+ \rangle$, the overlap region gives an uncertainty in $\langle 2_1^+ \| \hat{E}2 \| 2_1^+ \rangle$ of ± 0.067 eb. Similarly, if we assume no uncertainty in the Coulomb-excitation measurement, an uncertainty in $\langle 2_1^+ \| \hat{E}2 \| 2_1^+ \rangle$ of ± 0.050 eb is determined from the intersection of the dashed diagonal line with the lifetime limits; adding these two errors in quadrature yields ± 0.084 eb. Finally, on the k interval [0.6,1.0], $\langle 2_1^+ \| \hat{E}2 \| 2_1^+ \rangle = -0.108 \pm 0.0225$ eb, and adding the 0.0225 and 0.084 errors in quadrature gives the final $\langle 2_1^+ \| \hat{E}2 \| 2_1^+ \rangle = -0.110 \pm 0.087$ eb. Assuming an ideal rotor, $Q_S(2_1^+) = 0.75793 \langle 2_1^+ \| \hat{E}2 \| 2_1^+ \rangle$, we obtain a negative value of $Q_S(2_1^+) = -0.083 \pm 0.066$ eb.

New NCSM calculations with the CD-Bonn 2000 $2N$ potential of the transitional and diagonal matrix elements for the 2_1^+ and 2_2^+ states in ^{10}Be are presented in Fig. 5, as a function of the harmonic-oscillator frequency $\hbar\Omega$ and the size of the many-body model space $N_{\max}$. For the smallest model

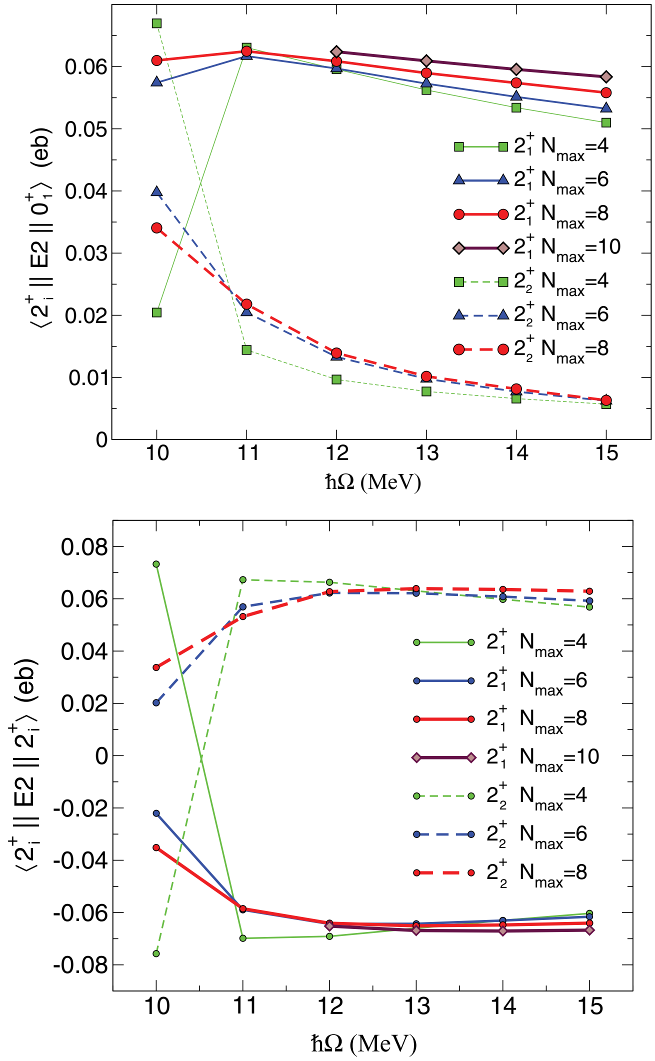

FIG. 5. (Color online) Calculated transitional (top panel) and diagonal (bottom panel) matrix elements involving the first two $J^\pi = 2^+$ states using NCSM with the CD-Bonn 2000 $2N$ potential at different $\hbar\Omega$ and $N_{\max}$.

space, $N_{\max} = 4$, and lowest $\hbar\Omega = 10$ MeV, the spin-orbit interaction is underestimated and the NCSM results agree with GFMC calculations using only the AV_{18} potential. As $N_{\max}$ increases and/or $\hbar\Omega$ increases, the spin-orbit interaction becomes effectively stronger and the order of the levels is restored. As shown in Fig. 5, the magnitude of the 2_1^+ $E2$ matrix element increases with increasing $N_{\max}$. Clearly, $Q_S(2_1^+)_{\rm NCSM} < 0$ and $Q_S(2_2^+)_{\rm NCSM} > 0$, in agreement with GFMC calculations using $2N$ and $3N$ forces [16].

Infinite-space results will, however, be independent on the choice of $\hbar\Omega$. We employ this property to perform constrained polynomial fits [5,46] to all calculated data points at large model spaces. These yield $Q_S(2_1^+)_{\rm NCSM} = -0.059(5)$ eb, or $\langle 2_1^+ \| \hat{E}2 \| 2_1^+ \rangle_{\rm NCSM} = -0.078(7)$ eb, and $B(E2; 2_1^+ \rightarrow 0_1^+)_{\rm NCSM} = 9.8(4)$ e^2fm^4, or $\langle 2_1^+ \| \hat{E}2 \| 0_1^+ \rangle_{\rm NCSM} = 0.0700(14)$ eb. These results are in agreement with the experimental data and recent no-core Monte Carlo shell-model [47] and GFMC [16] calculations. The inclusion of

$3N$ forces in the NCSM calculations was not investigated because of computational limitations at large model spaces.

In summary, we have demonstrated the feasibility of reorientation-effect Coulomb-excitation studies of high-lying 2_1^+ states in light nuclei using accelerated radioactive ion beams and a high-efficiency γ-ray spectrometer such as TIGRESS. This work assigns a negative sign to the $\langle 2_1^+ \| \hat{E}2 \| 2_1^+ \rangle$ diagonal matrix element in ^{10}Be. A more precise measurement requires higher statistics for the population of the 2_1^+ state as well as the measurement of the $k(2_1^+)$ polarizability parameter. Assuming an ideal rotor, $Q_S(2_1^+) < 0$; we are in agreement with *ab initio* calculations based on large-basis NCSM calculations with the CD-Bonn 2000 $2N$ potential and GFMC calculations including $3N$ forces in the full Hamiltonian. Such experiments play an important role in achieving a deeper understanding of the contributions of $2N$ and $3N$ potentials to the nuclear spin-orbit interaction, and how these contributions affect electric-quadrupole matrix elements motivates further experimental, as well as theoretical, investigations in this region of light nuclei.

J.N.O. thanks D. Cline, T. Davinson, A. M. Hurst, C. J. Lister, and D. H. Wilkinson for physics discussions. A.B.H. acknowledges funding by the NSF. C.F. acknowledges financial support from the European Research Council under the FP7. This work has been partially supported by the Natural Sciences and Engineering Research Council of Canada. TRIUMF receives federal funding via a contribution agreement through the National Research Council of Canada. LLNL participants are supported by the US DOE contract no. DE-AC52-07NA27344.

[1] P. Navrátil *et al.*, J. Phys. G **36**, 083101 (2009).
[2] S. C. Pieper and R. B. Wiringa, Annu. Rev. Nucl. Part. Sci. **51**, 53 (2001).
[3] R. Roth *et al.*, Phys. Rev. Lett **107**, 072501 (2011).
[4] R. B. Wiringa and S. C. Pieper, Phys. Rev. Lett. **89**, 182501 (2002).
[5] C. Forssén *et al.*, Phys. Rev. C **79**, 021303(R) (2009).
[6] P. Mueller *et al.*, Phys. Rev. Lett. **99**, 252501 (2007).
[7] W. Nörtershäuser *et al.*, Phys. Rev. Lett. **102**, 062503 (2009).
[8] E. Caurier *et al.*, Phys. Rev. C **66**, 024314 (2002).
[9] C. Forssén *et al.*, Phys. Rev. C **71**, 044312 (2005).
[10] S. C. Pieper *et al.*, Phys. Rev. C **64**, 014001 (2001).
[11] P. Navrátil *et al.*, Phys. Rev. Lett. **99**, 042501 (2007).
[12] E. Epelbaum *et al.*, Phys. Rev. Lett. **106**, 192501 (2011).
[13] P. Navrátil and S. Quaglioni, Phys. Rev. Lett. **108**, 042503 (2012).
[14] S. C. Pieper, Nucl. Phys. A **751**, 516c (2005).
[15] E. A. McCutchan *et al.*, Phys. Rev. Lett. **103**, 192501 (2009).
[16] E. A. McCutchan *et al.*, Phys. Rev. C **86**, 014312 (2012).
[17] J. N. Orce *et al.*, in preparation.
[18] J. Lassen *et al.*, Hyperfine Interact. **162**, 69 (2005).
[19] C. E. Svensson *et al.*, J. Phys. G **31**, S1663 (2005).
[20] C. E. Svensson *et al.*, Nucl. Instrum. Methods Phys. Res. A **540**, 348 (2005).
[21] H. C. Scraggs *et al.*, Nucl. Instrum. Methods Phys. Res. A **543**, 431 (2005).
[22] M. A. Schumaker *et al.*, Phys. Rev. C **78**, 044321 (2008).
[23] M. A. Schumaker *et al.*, Phys. Rev. C **80**, 044325 (2009).
[24] J. F. Ziegler *et al.*, Nucl. Instrum. Methods Phys. Res. B **268**, 1818 (2010).
[25] O. Häusser, in *Nuclear Spectroscopy and Reactions C*, edited by J. Cerny (Academic, New York, 1974).
[26] R. H. Spear, Phys. Rep. **73**, 369 (1981).
[27] D. L. Disdier *et al.*, Phys. Rev. Lett. **27**, 1391 (1971).
[28] H.-G. Voelk and D. Fick, Nucl. Phys. A **530**, 475 (1991).
[29] O. Häusser *et al.*, Nucl. Phys. A **212**, 613 (1973).
[30] W. J. Vermeer *et al.*, Phys. Lett. B **122**, 23 (1983).
[31] W. J. Vermeer *et al.*, Aust. J. Phys. **35**, 283 (1982).
[32] T. Czosnyka *et al.*, Bull. Am. Phys. Soc. **28**, 745 (1983).
[33] K. Alder and A. Winther, *Electromagnetic Excitation* (North-Holland, Amsterdam, 1975).
[34] J. Eichler, Phys. Rev. **133**, B1162 (1964).
[35] A. Migdal, J. Exp. Theor. Phys. USSR **15**, 81 (1945).
[36] J. S. Levinger, Phys. Rev. **107**, 554 (1957).
[37] F. C. Barker, Aust. J. Phys. **35**, 291 (1982).
[38] R. Nathans and J. Halpern, Phys. Rev. **92**, 940 (1953).
[39] A. M. Hurst *et al.*, Phys. Rev. Lett. **98**, 072501 (2007).
[40] T. Kibédi *et al.*, Nucl. Instrum. Methods Phys. Res. A **589**, 202 (2008).
[41] C. Y. Wu *et al.*, Nucl. Phys. A **607**, 178 (1996).
[42] E. K. Warburton *et al.*, Phys. Rev. **148**, 1072 (1966).
[43] T. R. Fisher *et al.*, Phys. Rev. **176**, 1130 (1968).
[44] S. Raman, C. W. Nestor Jr., C. W. Nestor, and P. Tikkanen, At. Data Nucl. Data Tables **78**, 1 (2001).
[45] B. Singh, Nuclear Data Sheets **107**, 1531 (2006).
[46] C. Forssén *et al.*, Phys. Rev. C **77**, 024301 (2008).
[47] L. Liu, T. Otsuka, N. Shimizu, Y. Utsuno, and R. Roth, Phys. Rev. C **86**, 014302 (2012).